DOI: 10.18721/JPM.14304
UDC 004.94

AN INFLUENCE ANALYSIS OF CREEP AND PLASTICITY CHARACTERISTICS ON THE SPARK PLASMA SINTERING PROCESS

V.A. Borisenko[1], **A.S. Semenov**[1], **T. Wallmersperger**[2]

[1] Peter the Great St. Petersburg Polytechnic University,
St. Petersburg, Russian Federation;

[2] Dresden University of Technology,
Dresden, Germany

In the paper, the spark plasma sintering (SPS) process for metal particles has been simulated based on experimental data and using the finite element method in the thermo-electro-mechanical formulation with taking into account the temperature influence on parameters of materials (nickel and copper). A comparison of obtained results with experimental data made it possible to create a computational model of the SPS process, the model being convenient to evaluate the influence of creep and plasticity parameters on the size of the interparticle neck forming in SPS. It was found that the creep effect significantly dominated over the plasticity influence on the process of forming the sintering neck at high temperatures. In this case, the variation of creep parameters in simulation also actively affects the formation of the neck.

Keywords: spark plasma sintering, metal, finite-element modelling, plasticity, creep, coupled fields

Citation: Borisenko V.A., Semenov A.S., Wallmersperger T., An influence analysis of creep and plasticity characteristics on the spark plasma sintering process, St. Petersburg Polytechnical State University Journal. Physics and Mathematics. 14 (3) (2021) 47–59. DOI: 10.18721/JPM.14304

АНАЛИЗ ВЛИЯНИЯ ХАРАКТЕРИСТИК ПОЛЗУЧЕСТИ И ПЛАСТИЧНОСТИ НА ПРОЦЕСС ИСКРОВОГО ПЛАЗМЕННОГО СПЕКАНИЯ

В.А. Борисенко[1], **А.С. Семенов**[1], **Т. Вальмерспергер**[2]

[1] Санкт-Петербургский политехнический университет Петра Великого,
Санкт-Петербург, Российская Федерация;

[2] Технический университет Дрездена,
г. Дрезден, Германия

На основе экспериментальных данных в работе промоделирован процесс искрового плазменного спекания (ИПС) металлических частиц методом конечных элементов в термоэлектромеханической постановке с учетом влияния температуры на параметры материалов (никеля и меди). Сравнение результатов моделирования с экспериментом позволило создать вычислительную модель процесса ИПС, удобную для оценки влияния параметров ползучести и пластичности на размер межчастичной шейки, образующейся при проведении ИПС. Установлено, что для высоких температур эффект ползучести в несколько раз превосходит влияние пластичности на процесс образования шейки спекания. При этом изменение параметров ползучести при моделировании также активно влияет на формирование шейки.

Ключевые слова: искровое плазменное спекание, металл, конечно-элементное моделирование, пластичность, ползучесть, связанные поля

Ссылка при цитировании: Борисенко В.А., Семенов А.С., Вальмерспергер Т. Анализ влияния характеристик ползучести и пластичности на процесс искрового плазменного спекания // Научно-технические ведомости СПбГПУ. Физико-математические науки. 2021. Т. 14. № 3. С. 47–59. DOI: 10.18721/JPM.14304

Introduction

Detailed experimental and theoretical studies [1, 2], as well as simulations [3 – 5] have been carried out for sintering and compaction of powder metallurgy products, aimed at improving their properties. The technology for obtaining metal powders and manufacturing products from them offers several benefits [6, 7], in particular, making it possible to synthesize materials that are difficult or impossible to obtain by other methods; furthermore, it helps save metal and significantly reduces the production costs. Additionally, using pure starting powders yields sintered materials with a lower impurity content, better corresponding to a given composition compared to conventional cast alloys. Sintered materials have better mechanical properties compared to cast ones with the same composition and density; for instance, the preferred orientation of the crystal grains of the metal (texture), which is characteristic for cast equivalents, has a smaller adverse effect. The size and shape of the structural elements of sintered materials are easier to control, and even more importantly, it is possible to produce such types of mutual arrangement and shape of grains that are unattainable for cast metal.

Due to these structural peculiarities, sintered metals are more heat-resistant, better tolerate the effects of cyclic fluctuations in temperature and stress, as well as nuclear radiation, which is crucial for the materials used in novel devices.

Spark Plasma Sintering/Field Assisted Sintering Technology (SPS/FAST) is an effective method for obtaining defect-free blanks from powder materials, combining pressing with an intense electrical discharge, allowing to obtain compact materials in a very short time. Recently, there has been an increase in the number of studies on spark plasma sintering (see, for example, [11 – 13]). The essence of this method for consolidating powder materials is that substances are heated by electric current pulses passing through it. This way, the temperature and sintering time are greatly reduced compared to conventional high-temperature sintering and hot pressing.

The difficulties with simulating the given class of problems are due to different sintering mechanisms (plasticity, creep, thermal migration, etc.). In addition, the sintering process consists of multiple pronounced stages: neck growth, formation and subsequent shrinkage of closed pores. Moreover, fields of different nature interact in this case: electrical, thermal, chemical and mechanical. The nontrivial dependence of electrical and mechanical constants on the temperature of the material can cause problems with the convergence of the solution during simulation. This convergence also strongly depends on the parameters of the contact, namely the thermal and electrical conductivity of the zone of contacting elements. Finite element modeling (FEM) is a valuable tool for gaining a better understanding of the process. FEM was mainly used previously to study macroscopic temperature gradients in samples during a fast process [14 – 16] but recently more and more works [4, 5] consider FEM of particle deformation, as well as microscopic distribution of current and temperature upon particle contact as the simplest representative volume of powder.

It was established in [5] that using elastic and viscoelastic models of the sintered material in simulating such processes does not yield a good correlation with experimental data. In this case, the best accuracy was obtained by simultaneously taking into account both viscous and plastic effects.

The goal of this study consisted in analyzing the potential offered by FEM of spark plasma sintering by comparing the results with experimental data.

To solve this problem, it was necessary to analyze the influence of a number of key factors and, first of all, creep, on the diameter of the interparticle neck formed in the process of the studied technology.

Experimental setup and mathematical model

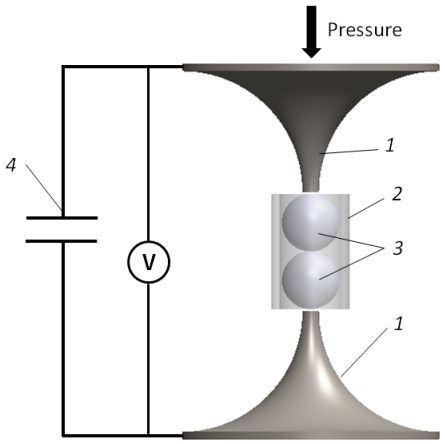

Fig. 1. Schematic of experimental setup: copper punches *1*, thick-walled glass tube *2*, nickel balls *3*, electrolytic capacitors *4*

The experiments carried out at the Dresden University of Technology (Germany) [4, 5] involved balls made of commercially pure nickel 1 mm in diameter. To remove oxides from nickel spheres, the balls were placed in a citric acid solution for several hours and rinsed with distilled water and ethanol before they were inserted into the setup. An experimental setup was developed and built specifically to study the initial stages of contact formation under spark plasma sintering. The diagram is shown in Fig. 1.

Copper punches *1* 1 mm in a diameter are located at the top and bottom of the setup. Thick-walled glass tube *2* with a 1 mm internal diameter is attached to the lower punch to prevent balls *3* from falling out. Two nickel balls are placed between the fitting punches. A mechanical load (Pressure) is applied to the upper punch using a 1 kg weight providing an axial compressive force of 12.5 MPa in the cross section of the copper punches, and, accordingly, in the equatorial section of the balls. An electrode containing two series-connected electrolytic capacitors *4* is attached to the upper punch. The second electrodes of the capacitor are connected to the lower punch via a current rectifier that serves as a switch controlled by a microcontroller. The capacitors were charged to a voltage from 1 to 8 V (the value depended on the experimental conditions).

Mathematical model

We consider a related thermoelectromechanical axisymmetric problem for analyzing the deformations, emerging stresses, as well as the evolution of the temperature field and contact resistance. Elastic, plastic and viscous parameters of the material are used for simulating the mechanical component of the problem. Given that there are no reliable data for nickel plasticity curves at high temperatures, a plasticity model with linear hardening was used to simulate plastic deformations. The von Mises condition was considered as a condition for the onset of plasticity, due to the isotropy of the material. The heat balance equation taking into account the Fourier law was used for non-stationary processes accompanying the changes in the thermal field.

The complete system of equations for a coupled thermoelectromechanical initial boundary-value problem has the following form for the given conditions:

$$\begin{cases} \rho(T)C(T)\dfrac{\partial T}{\partial t} - \nabla\cdot\left(\lambda(T)\,\mathbf{E}\cdot\nabla T\right) - q_v = 0, \\ \nabla\cdot\left({}^4\mathbf{C}(T)\cdot\cdot\left((\nabla\mathbf{u})^s - \boldsymbol{\alpha}(T)\left(T - T_{ref}\right) - \boldsymbol{\varepsilon}^P - \boldsymbol{\varepsilon}^c\right)\right) = 0, \\ \nabla\cdot\left(\boldsymbol{\varepsilon}_n\cdot\nabla\dfrac{\partial\varphi}{\partial t}\right) + \nabla\cdot\left[\boldsymbol{\sigma}(T)\cdot\nabla\varphi\right] = 0, \end{cases} \quad (1)$$

where λ is the thermal conductivity, T is the temperature, T_{ref} is the initial temperature, $\boldsymbol{\varepsilon}^P$ is the plastic deformation tensor, $\boldsymbol{\varepsilon}^c$ is the deformation creep, ρ is the density, C is the specific heat, q_v is the volumetric heat transfer, φ is the scalar electric potential, $\boldsymbol{\sigma}$ is the electrical conductivity tensor, ε_p the dielectric permittivity tensor of the medium, $\mathbf{f}_v$ is the volumetric force vector, $\mathbf{u}$ is the displacement vector, $^4\mathbf{C}$ is the stiffness tensor, $\boldsymbol{\alpha}$ is the tensor of linear thermal expansion coefficients.

Volume forces and inertial terms are absent from the equilibrium equation of system (1) in the given problem statement. The values of elastic, thermal and electrical constants of the material depending on temperature are given in Table 1 for nickel and copper (taken from [4, 5]); the dimensions of the given constants correspond to a certain system of units: millimeters, gigagrams, seconds (mm, Gg, s). Table 1 also lists the values of the yield stress σ_y and the plastic modulus H_0 corresponding to the model of plasticity with linear hardening. The data presented indicate that the characteristics of materials are considerably dependent on temperature. In SPS, a current passing through the material causes it to heat up, leading to a change in the material constants, for example, resistivity. A change in the latter in turn leads to a change in the current and density of the heat released in the given section. This chain reflects how the material constants are related to the temperature field, and how, in turn, the temperature field depends on these constants.

Norton's law based on the similarity hypothesis was used to account for creep. In general, Norton's law is written as

$$\boldsymbol{\varepsilon}^c = A\sigma_i^{n-1}\mathbf{S}\cdot t\cdot\exp\left(-\frac{\Delta H}{RT}\right), \tag{2}$$

where ΔH is the creep activation energy; R is the Boltzmann constant; t is the time; T is the temperature; σ is the stress; n and A are the power and linear creep indicators; $\mathbf{S}$ is the stress tensor deviator.

The values of the creep constants were taken from monograph [17]:

$A = 80.4$ MPa$^{-4.6}$/s, $n = 4.6$, $\Delta H = 284$ kJ for nickel;

$A = 2.45$ MPa$^{-4.8}$/s, $n = 4.8$, $\Delta H = 197$ kJ for copper.

Since the problem is symmetric with respect to the contact plane of the balls, it seems reasonable to consider only the upper part of the structure in the FE simulation (see Fig. 1); it is shown in a horizontal position in Fig. 2, *a*,*b*. The FE model is shown in Fig. 2,*a*. It contains 1524 elements and 4491 nodes. The model was constructed in the ANSYS FEA package using PLANE 223 type elements in a thermoelectromechanical setting.

The contact between the balls in this symmetric statement is modeled as the contact between the upper ball and an absolutely rigid plane. Since boundary conditions in the given problem should be imposed taking into account the experimental procedure, they should be mechanical, electrical and thermal in nature. The mechanical component should reflect the restricted displacements and the fact that pressure is applied to the upper copper punch. A restriction on displacement of the contact surface was imposed in the symmetric problem statement. The electrical component accounted for the potential difference applied to the electrodes of the test setup. The function of the potential over time was taken to be equal to half the voltage between the capacitor plates changing over time. An exponential curve was combined with its piecewise-linear point approximation for the FE simulation (Fig. 2,*c*).

The following boundary conditions were imposed on the free surface of the ball and the punch: zero normal stress and electric current ($\sigma_n = 0$, $J_n = 0$), thermal radiation by the Stefan – Boltzmann law (the ball material was assumed to be a blackbody with the emissivity $\varepsilon = 1$) $q_n = \varepsilon\cdot\sigma_{SB}\cdot\left(T^4 - T_0^4\right)$. Restrictions on the radial components of displacement, electric current and heat flux were imposed on the boundary of axial symmetry: $u_n = 0$, $J_n = 0$, $q_n = 0$. The boundary conditions of zero displacement, potential and heat flux were imposed on the contact boundary of the balls: $u_n = 0$, $\varphi = 0$, $q_n = 0$.

Table 1

Values of elastic, thermal and electrical constants of nickel and copper depending on temperature [4, 5]

T, K (^{o}C)	300 (27)	500 (227)	700 (427)	900 (627)	1100 (827)	1400 (1127)	1728 (1455)
Values for nickel							
ρ, Gg/mm^3	8.90e–12	8.82e–12	8.74e–12	8.65e–12	8.55e–12	8.40e–12	8.10e–12
C_p, J/(Gg·K)	4.44e+8	5.24e+8	5.24e+8	5.43e+8	5.77e+8	6.09e+8	6.25e+8
λ, W/(mm·K)	0.0904	0.0721	0.0609	0.0662	0.0735	0.0767	0.0785
ρ_e, Ω·mm	7.37e–5	18.0e–5	32.0e–5	38.7e–5	44.5e–5	52.4e–5	59.0e–5
α, 1/K	13e–6	14e–6	15e–6	16.5e–6	17e–6	19e–6	13e–6
E, GPa	218	199	195	192	171	141	–
ν	0.28	0.28	0.28	0.30	0.31	0.34	–
σ_y, MPa	185	180	140	80	50	–	–
H_0, MPa	1800	1400	1100	1000	750	–	–
Values for copper							
ρ, Gg/mm^3	8.93e–12	8.63e–12	8.73e–12	8.62e–12	8.51e–12	8.39e–12	7.96e–12
C_p, J/(Gg·K)	3.85e+8	4.08e+8	4.25e+8	4.41e+8	4.64e+8	5.07e+8	5.14e+8
λ, W/(mm·K)	0.402	0.385	0.370	0.355	0.338	0.322	0.184
ρ_e, Ω·mm	1.73e–5	3.09e–5	4.51e–5	6.04e–5	7.72e–5	9.59e–5	23.4e–5
α, 1/K	16e–6	18e–6	19e–6	20e–6	24e–6	29e–6	–
E, GPa	130	115	103	89.7	76.8	63.7	–
ν	0.35	0.35	0.35	0.36	0.38	0.40	–
σ_y, MPa	220	190	100	40	–	–	–
H_0, MPa	500	400	200	200	–	–	–

Notations: T is the temperature, ρ is the density, C_p is the heat capacity at constant pressure, λ is the thermal conductivity, ρ_e is the resistivity, α is the thermal expansion coefficient, E is Young's modulus, ν is Poisson's ratio, σ_y is the yield stress, H_0 is the plastic modulus.

The following boundary conditions were imposed on the upper boundary of the punch: pressure versus time $\sigma_n = p(t)$, potential versus time $\varphi = V(t)/2$ and initial temperature $T = T_0$. The general form of the boundary conditions is shown in Fig. 2,*b*.

The penalty function method was used. The following parameter values were given:

normal contact stiffness factor equal to 1.0;

penetration tolerance factor equal to 0.1;

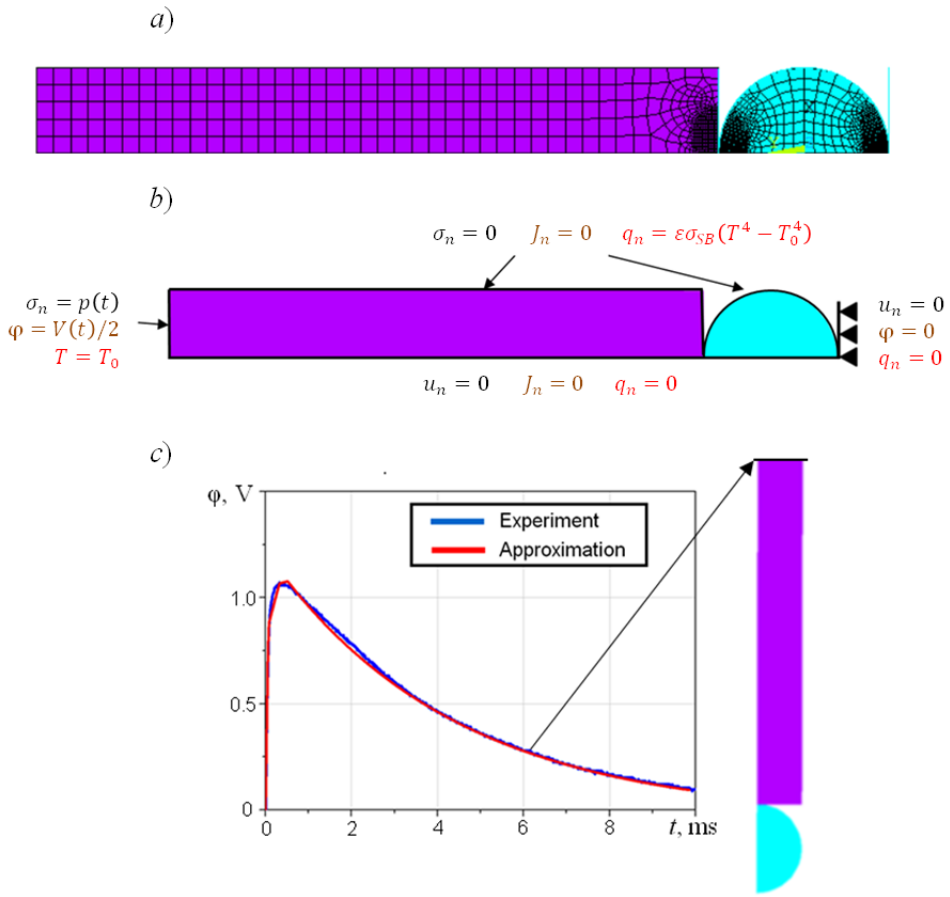

Fig. 2. Schematic representation of FE model
of spark plasma sintering for copper punch (purple) and nickel ball (blue):
a corresponds to partition of objects into finite elements, *b* illustrates the boundary conditions
of the problem statement, *c* is the graph of the electric potential applied to the upper boundary of the punch

thermal contact conductivity equal to 1 kW/K;
electrical contact conductivity equal to 1 MS.

Computational results and discussion

A series of simulations by the finite element method was performed to assess the influence of the yield parameters on the results of SPS. Virtual experiments differed by the initial charge of the capacitor and, accordingly, the dependence of the passing current on time. We selected three cases of initial voltage on the capacitor before the start of the SPS process were chosen: 2, 3, and 5 V. The input data for the mathematical model was the dependence of the voltage in the setup on time, recorded in a real experiment. The creep parameters were varied in addition to the change in the initial voltage on the capacitor plates, namely, its power exponent n and its activation energy ΔH.

We only analyzed the results obtained for the first 10 ms of the computational experiment, since the main changes in the thermal and electric fields were basically finished by the end of this time interval, and the process was observed to reach steady behavior.

The problem was solved in two thermoelectromechanical statements to assess the effect of creep on the temperature of the interparticle neck during sintering: without creep and taking it into account. The results obtained in [4] were used for verification, where the FE model was considered in a thermoelectric statement without mechanical deformations taken into account. The radius of the neck

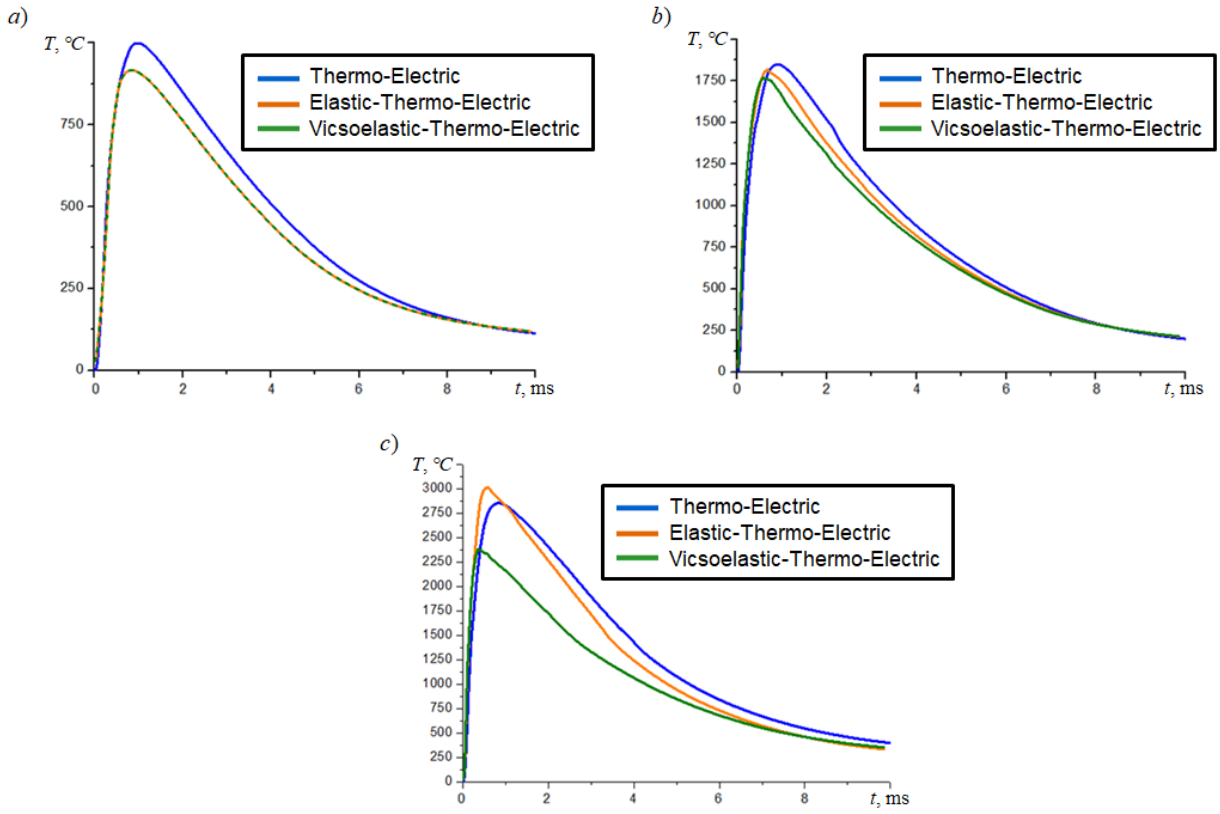

Fig. 3. Comparison of temperature evolution in the interparticle neck at initial voltages on capacitor plates equal to 2 V (*a*), 3 V (*b*) and 5 V (*c*), obtained in two thermoelectromechanical statements and compared with the thermoelectric statement (blue curves) [4]

contact was set in this model according to the experimental results and did not change throughout the entire simulation.

The graphs below are given for the dependence of the temperature of the neck material on time during sintering for three experiments differing in the initial voltage on the capacitor plates: 2, 3, and 5 V (Fig. 3). Apparently, accounting for creep at an initial voltage of 2 V does not affect the temperature change.

In addition, we compared the diameters of the sintering neck for the computational cases with and without accounting for the creep of its material, with different initial voltages on the capacitor plates (Table 2). The maximum diameter of the contact between spherical particles was taken as the neck diameter in the mathematical model.

Analyzing the data in Table 2, we can conclude that accounting for the creep at high initial voltages on the capacitor plates (3 and 5 V) makes it possible to refine the neck diameter and approach the experimental data, while the magnitude of the creep practically does not affect the growth of the neck at low temperatures.

The effect of creep at a high temperature provides a large area of contact between the particles, and, therefore, the peak temperature is lower. This result is consistent with the dependences shown in Fig. 4.

Significant differences between the simulation results and experimental data can be explained by increasing influence of other factors governing the formation of the interparticle neck, for example, the phenomena of surface and grain-boundary diffusion, which can develop at high capacitor volt-

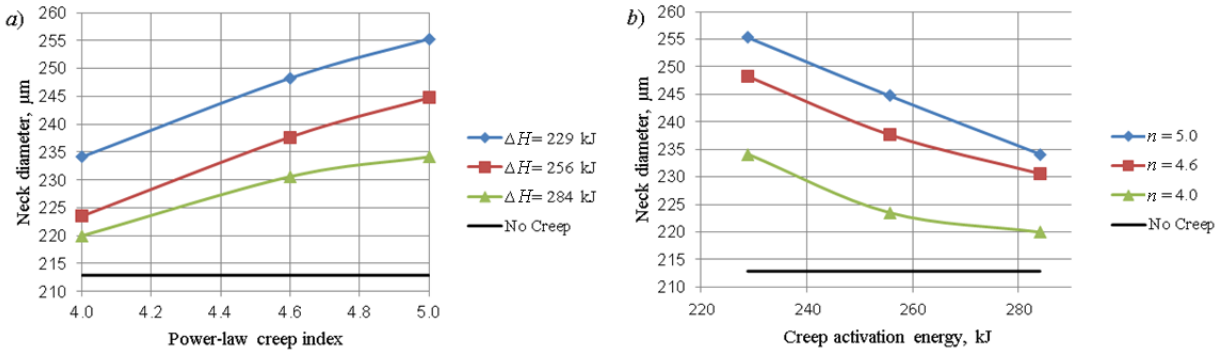

Fig. 4. Neck diameter depending on creep exponent n (*a*) and creep activation energy ΔH (*b*)

Table 2

Comparison of diameters of interparticle neck in spark plasma sintering, obtained experimentally and by the FEM method

Method	Neck diameter, μm			Deviation, %		
	2 B $T = 258$ K	3 B	5 B	2 B $T = 258$ K	3 B	5 B
		$T = 267$ K			$T = 267$ K	
Experiment	148	171	293	–		
FEM in elastic statement	147	158	213	–0.7	–7.6	–27
FEM accounting for creep	147	164	227	–0.7	–4.1	–23

Notes. 1. Data are given for three values of the initial voltage on the capacitor plates and two values of temperature.
2. Deviations of the computed results from the experiment are shown.

ages, and, consequently, with greater heating. Unfortunately, such effects are not implemented yet in the ANSYS FEA package.

To assess the influence of necking mechanisms, we considered the dependence of plastic and creeping deformations on the voltage set on the capacitor plates (Fig. 5). Analysis of the dependences plotted confirms that plasticity is the main mechanism behind the formation of an interparticle neck at low capacitor voltages before discharge (which is equivalent to a lower current passing through the system), while the main factor at higher voltages is creep.

Because creep has a considerable influence on the processes occurring at high initial voltages V on the capacitor plates, we estimated the influence of the parameters of the Norton creep law on the obtained diameter of the sintering neck was estimated for a value $V = 5$ V. The following set of parameters of Norton's creep law was selected:

the values $n = 5$ and 4 corresponding to deviations of +9 and –13% from the initial tabular value were taken for the creep exponent n, in addition to the tabular value $n = 4.6$ [17];

the values $\Delta H = 255.6$ and 228.9 kJ corresponding to deviations of 10 and 20% from the initial tabular value were taken for the creep activation energy ΔH, in addition to the tabular value $\Delta H =$ = 284 kJ [17].

The dependences for neck diameter on the creep exponent n and creep activation energy ΔH are shown in Fig. 4.

In addition to the above, we estimated the influence of the yield stress on the resulting neck size for the given tabular values of the creep parameters $n = 4.6$ and $\Delta H = 284$ kJ [17]. The following values of the yield stress (in MPa) were taken: 160, 180, 200, 220 and 240. The resulting dependence of the

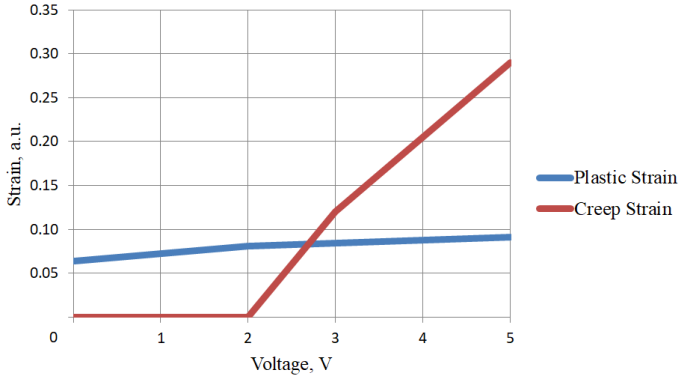

Fig. 5. Levels of plastic and creeping deformations
in the SPS interparticle neck depending on voltage on the capacitor plates

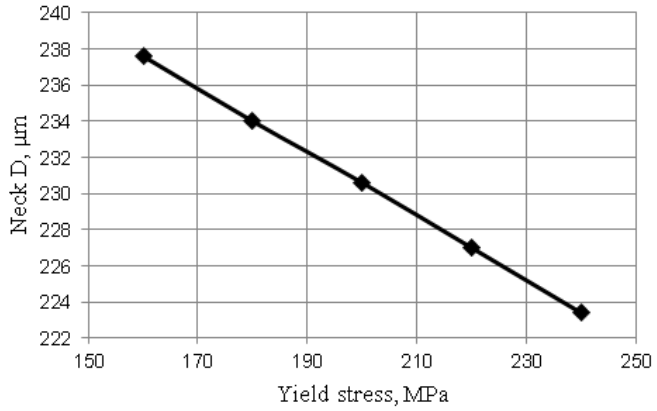

Fig. 6. Sintering neck diameter depending on yield stress of the ball material

sintering neck diameter on the yield stress is shown in Fig. 6. Evidently, the nature of the plotted dependence is actually linear for the given parameter values.

It was found that a 9% increase in the exponent results in an increase in the neck diameter by 3%, while taking into account the contribution of creep deformations results in an increase in the neck diameter by 50%. At the same time, its decrease by 13% leads to a decrease in the neck diameter by 3.1%. Furthermore, a decrease in the creep activation energy ΔH by 10% leads to an increase in the neck diameter by 5%, and taking into account the contribution of creep deformations to an increase in the neck diameter by 75%; a decrease in ΔH by 20% leads to an increase in the neck diameter by 10%, and taking into account the contribution of creep deformations to an increase in the neck diameter by 150%. In addition, a 20% increase in the yield stress results in a 3% decrease in the neck diameter.

These dependences confirm our conclusions about the predominant contribution of creeping deformations to the SPS process, in comparison with the influence of plastic deformations.

Conclusion

Based on the results obtained, we can argue that the behavior of sintered particles can be described fairly satisfactorily for low voltages on capacitor plates during spark plasma sintering. However, if higher voltages are set, the given thermoelectromechanical concepts of microparticle sintering mechanisms turn out to be insufficient for reliably modeling this process.

It was found that the creep effect on the sintering neck growth is several times greater for high temperatures than the effect of plasticity. At the same time, the change in the creep parameters during modeling also actively affects the formation of the neck. A deviation of the creep activation energy from the tabulated values by only 10% can produce an increase in creep deformations by 75% and an increase in neck diameter by 5%.

According to the data in monograph [18], the diffusion mechanism has a major effect on the sintering process along with the creep phenomenon. The influence of high temperatures (over 1500 °C) on the process of grain-boundary and surface diffusion was estimated in [19, 20].

Accounting for these necking mechanisms as well as creep and plasticity can give a more accurate agreement between the simulated results for high-current sintering and the available experimental data.

REFERENCES

1. **Anselmi-Tamburini U., Garay J.E., Munir Z.A.,** Fundamental investigations on the spark plasma sintering/synthesis process: III. Current effect on reactivity, Mater. Sci. Eng. A. 407 (1–2) (2005) 24–30.

2. **Trapp J., Semenov A.S., Nöthe M., et al.,** Fundamental principles of spark plasma sintering of metals: part III – densification by plasticity and creep deformation, Powder Metallurgy. 63 (5) (2020) 329–337.

3. **Wei Li,** Constitutive modeling and simulation of spark plasma sintering with applications to fabrication of functionally structured mono-carbides, Ph. D. thesis, University of California, San Diego, USA, 2013.

4. **Semenov A.S., Trapp J., Nöthe M., et al.,** Experimental and numerical analysis of the initial stage of field-assisted sintering of metals, J. Mater. Sci. 52 (3) (2017) 1486–1500.

5. **Semenov A.S., Trapp J., Nöthe M., et al.,** Thermo-electro-mechanical modeling, simulation and experiments of field-assisted sintering, J. Mater. Sci. 54 (15) (2019) 10764–10783.

6. **Barinov V.Yu., Rogachev A.S., Vadchenko S.G., et al.,** Iskrovoye plazmennoye spekaniye izdeliy slozhnoy formy s ispolzovaniyem kvaziistaticheskogo pressovaniya [Spark plasma sintering of complex-shaped products using quasi-static pressing], Mezhdunarodnyy zhurnal prikladnykh i fundamentalnykh issledovaniy [International Journal of Applied and Fundamental Research]. (1-3) (2016) 312–315 (in Russian).

7. **Grigoryev E.G., Kalin B.A.,** Elektroimpulsnaya tekhnologiya formirovaniya materialov iz poroshkov [Spark-discharge technology of material forming from powders], Moscow Engineering and Physical Institute (MEPhI), Moscow, 2008 (in Russian).

8. **Kolerov O.K.,** Characteristics of primary recrystallization and its role in the sintering of metal powders, Soviet Powder Metallurgy and Metal Ceramics. 12 (3) (1973) 192–195.

9. **Petrushina M.V., Pogudo E.L., Chivel Yu.A.,** Simulation of the process of sintering of spherical powders under the effect of pulsed laser radiation, High Temperature. 44 (1) (2006) 151–155.

10. **Mishra D.D., Agarwala V., Agarwala R.C.** Sintering behavior of mechanically alloyed Ti-48Al-2Nb aluminides, High Temperature. 52 (1) (2014) 65–71.

11. **Maniere C., Durand L., Weibel A., Estournes C.,** Spark plasma sintering and finite element method: from the identification of the sintering parameters of a submicronic α-alumina powder to the development of complex shapes, Acta Materialia. 102 (1 January) (2016) 169–175.

12. **Munir Z.A., Anselmi-Tamburini U., Ohyanagi M.,** The effect of electric field and pressure on the synthesis and consolidation of materials: a review of the spark plasma sintering method, J. Mater. Sci. 41 (3) (2006) 763–777.

13. **Olevsky E., Froyen L.,** Constitutive modeling of spark-plasma sintering of conductive materials, Scripta Materialia. 55 (12) (2006) 1175–1178.

14. **Orru R., Licheri R., Locci A.M., et al.,** Consolidation/synthesis of materials by electric current activated/assisted sintering, Mater. Sci. Eng. R: Reports. 63 (4–6) (2009) 127–287.

15. **Allen J., Walter C.,** Numerical simulation of the temperature and stress field evolution applied to the field assisted sintering technique, ISRN Mater. Sci. 2012 (2012) ID 698158. 1–9.

16. **Zinoviev V.E.,** Teplofizicheskiye svoystva metallov pri vysokikh temperaturakh [Thermophysical properties of metals at high temperatures (Handbook)], Metalurgia, Moscow, 1989 (in Russian).

17. **Frost H.J., Ashby M.F.,** Deformation-mechanism maps: the plasticity and creep of metals and ceramics, Pergamon Press, Oxford [Oxfordshire], New York, 1982.

18. **Kang S.-J. L.,** Sintering: densification, grain growth and microstructure, Elsevier Butterworth-Heinemann, 2005.

19. **Borisenko V.A., Semenov A.S.,** Issledovaniye deformirovaniya mezhchastichnoy sheyki metallicheskikh mikrochastits putem diffuzii [Studies in straining the interparticle neck of metal microparticles through diffusion], SPbPU Science Week, Materials of Scientific Conference with International Participation, November 13–19, 2017, Institute of Applied Mathematics and Mechanics, Polytechnical Institute Publishing, St. Petersburg (2017) 103–105 (in Russian).

20. **Borisenko V.A., Semenov A.S.,** Modelirovaniye protsessa rosta sheyki mezhdu dvumya sfericheskimi chastitsami pri spekanii [Simulation of the process of a neck growth between two spherical particles during sintering], SPbPU Science Week, Materials of Scientific Conference with International Participation, November 19–24, 2018, Institute of Applied Mathematics and Mechanics, Polytechnical Institute Publishing, St. Petersburg (2018) 80–83 (in Russian).

Received 13.04.2021, accepted 18.06.2021.

THE AUTHORS

BORISENKO Vladislav A.
Peter the Great St. Petersburg Polytechnic University
29 Politechnicheskaya St., St. Petersburg, 195251, Russian Federation
vladborisenko1995@gmail.com

SEMENOV Artem S.
Peter the Great St. Petersburg Polytechnic University
29 Politechnicheskaya St., St. Petersburg, 195251, Russian Federation
Semenov.Artem@googlemail.com

WALLMERSPERGER Thomas
Dresden University of Technology
3c, George-Bähr-Straße, Dresden, 01069, Saxony, Germany
servicecenter.studium@tu-dresden.de

СПИСОК ЛИТЕРАТУРЫ

1. **Anselmi-Tamburini U., Garay J.E., Munir Z.A.** Fundamental investigations on the spark plasma sintering/synthesis process: III. Current effect on reactivity// Materials Science and Engineering. A. 2005. Vol. 407. No. 1–2. Pp. 24–30.

2. **Trapp J., Semenov A.S., Nöthe M., Wallmersperger T., Kieback B.** Fundamental principles of spark plasma sintering of metals: part III – densification by plasticity and creep deformation // Powder Metallurgy. 2020. Vol. 63. No. 5. Pp. 329–337.

3. **Wei Li.** Constitutive modeling and simulation of spark plasma sintering with applications to fabrication of functionally structured mono-carbides. Ph. D. thesis. San Diego, USA: University of California, 2013. 271 p.

4. **Semenov A.S., Trapp J., Nöthe M., Eberhardt O., Wallmersperger T., Kieback B.** Experimental and numerical analysis of the initial stage of field-assisted sintering of metals // Journal of Materials Science. 2017. Vol. 52. No. 3. Pp. 1486–1500.

5. **Semenov A.S., Trapp J., Nöthe M., Eberhardt O., Wallmersperger T., Kieback B.** Thermo-electro-mechanical modeling, simulation and experiments of field-assisted sintering // Journal of Materials Science. 2019. Vol. 54. No. 15. Pp. 10764–10783.

6. **Баринов В.Ю., Рогачев А.С., Вадченко С.Г., Московских Д.О., Колобов Ю.Р.** Искровое плазменное спекание изделий сложной формы с использованием квазистатического прессования // Международный журнал прикладных и фундаментальных исследований. 2016. № 1-3. С. 312–315.

7. **Григорьев Е.Г., Калин Б.А.** Электроимпульсная технология формирования материалов из порошков. М.: Изд-во МИФИ, 2008. 152 с.

8. **Колеров О.К.** Особенности первичной рекристаллизации и ее роль при спекании металлических порошков // Порошковая металлургия. 1973. № 3. С. 18–22.

9. **Петрушина М.В., Погудо Е.Л., Чивель Ю.А.** Моделирование процесса спекания сферических порошков под действием импульсного лазерного излучения // Теплофизика высоких температур. 2006. Т. 44. № 1. С. 148–152.

10. **Mishra D.D., Agarwala V., Agarwala R.C.** Sintering behavior of mechanically alloyed Ti-48Al-2Nb aluminides // Теплофизика высоких температур. 2014. Т. 52. № 1. С. 65–71.

11. **Maniere C., Durand L., Weibel A., Estournes C.** Spark plasma sintering and finite element method: from the identification of the sintering parameters of a submicronic α-alumina powder to the development of complex shapes // Acta Materialia. 2016. Vol. 102. 1 January. Pp. 169–175.

12. **Munir Z.A., Anselmi-Tamburini U., Ohyanagi M.** The effect of electric field and pressure on the synthesis and consolidation of materials: a review of the spark plasma sintering method // Journal of Materials Science. 2006. Vol. 41. No. 3. Pp. 763–777.

13. **Olevsky E., Froyen L.** Constitutive modeling of spark-plasma sintering of conductive materials // Scripta Materialia. 2006. Vol. 55. No. 12. Pp. 1175–1178.

14. **Orru R., Licheri R., Locci A.M., Cincotti A., Cao G.** Consolidation/synthesis of materials by electric current activated/assisted sintering // Materials Science and Engineering. R: Reports. 2009. Vol. 63. No. 4–6. Pp. 127–287.

15. **Allen J., Walter C.** Numerical simulation of the temperature and stress field evolution applied to the field assisted sintering technique // ISRN Materials Science. 2012. Vol. 2012. Article ID 698158. Pp. 1–9.

16. **Зиновьев В.Е.** Теплофизические свойства металлов при высоких температурах. М.: Металлургия, 1989. 384 с.

17. **Фрост Г.Дж., Эшби М.Ф.** Карты механизмов деформации. Пер. с англ. Челябинск: Металлургия, 1989. 328 с.

18. **Kang S.-J.L.** Sintering: densification, grain growth and microstructure. Oxford: Elsevier Butterworth-Heinemann, 2005. 265 p.

19. **Борисенко В.А., Семенов А.С.** Исследование деформирования межчастичной шейки металлических микрочастиц путем диффузии // Неделя науки СПбПУ. Материалы научной конференции с международным участием. Институт прикладной математики и механики. 13–19 ноября 2017 г., СПб.: Изд-во Политехн. ун-та, 2017. С. 103–105.

20. **Борисенко В.А., Семенов А.С.** Моделирование процесса роста шейки между двумя сферическими частицами при спекании // Неделя науки СПбПУ. Материалы научной конференции с международным участием. Институт прикладной математики и механики. 19–24 ноября 2018 г., СПб.: Изд-во Политехн. ун-та, 2018. С. 80–83.

Статья поступила в редакцию 13.04.2021, принята к публикации 18.06.2021.

СВЕДЕНИЯ ОБ АВТОРАХ

БОРИСЕНКО Владислав Андреевич – *инженер-исследователь Института передовых производственных технологий Санкт-Петербургского политехнического университета Петра Великого, Санкт-Петербург, Российская Федерация.*

195251, Российская Федерация, г. Санкт-Петербург, Политехническая ул., 29

vladborisenko1995@gmail.com

СЕМЕНОВ Артем Семенович – *кандидат физико-математических наук, доцент Высшей школы механики и процессов управления, заведующий кафедрой сопротивления материалов Санкт-Петербургского политехнического университета Петра Великого, Санкт-Петербург, Российская Федерация.*

195251, Российская Федерация, г. Санкт-Петербург, Политехническая ул., 29

Semenov.Artem@googlemail.com

ВАЛЬМЕРСПЕРГЕР Томас – *доктор технических наук, профессор Технического университета Дрездена, г. Дрезден, Саксония, Германия.*

01062, Германия, г. Дрезден

servicecenter.studium@tu-dresden.de